Electrode Materials

DOI: 10.1002/anie.201309641

Reversible Self-Assembly of Terpyridine-Functionalized Graphene Oxide for Energy Conversion**

Shungang Song, Yuhua Xue, Lianfang Feng, Hany Elbatal, Pingshan Wang, Charles N. Moorefield, George R. Newkome, and Liming Dai**

Abstract: *Terpyridine-functionalized graphene oxides were prepared for self-assembly into 3D architectures with various metal ions (e.g., Fe, Ru). The resulting electrode materials showed significantly improved electroactivities for efficient energy conversion and storage. They showed promise for application in the oxygen reduction reaction (ORR), photocurrent generation, and supercapacitance.*

Owing to its excellent optical, thermal, mechanical, and electric properties, graphene has attracted considerable interest for a large variety of potential applications.[1] However, graphene sheets without functionalization are insoluble and infusible, which has limited their large-scale practical application. The covalent and/or noncovalent functionalization of graphene with various soluble moieties (metal or metal-oxide nanoparticles) has been widely reported to improve its processibility (catalytic activity).[2–5] Although most of the reported covalent reactions for the functionalization of graphene have improved its processibility to facilitate applications, they often cause permanent structural/property changes. For many applications (e.g., tunable electronic and optical devices), the controllable and reversible functionalization of graphene and its derivatives is highly desirable. Such functionalization would not only increase our understanding of structure–property relationships, but would also lead to various multifunctional self-assemblies of the functionalized graphene for novel applications.

Self-assembly is often driven by hydrogen-bonding, electrostatic, and/or π–π stacking interactions.[6] However, the complexation of 2,2′:6′,2″-terpyridine and its derivatives with certain metal ions[7] has also been utilized for the reversible self-assembly of small molecules,[8] polymers,[9] and even carbon nanotubes.[10] As compared to other complexation ligands (e.g., 2,2′-bipyridine and 1,10-phenanthroline), terpyridine complexes are often achiral and shape-controllable[11] with excellent optical and electrochemical properties. As far as we are aware, however, neither terpyridine-functionalized graphene nor the terpyridine-assisted self-assembly of graphene through metal complexation has been reported. In the present study, we designed and synthesized a class of terpyridine-functionalized graphene oxides (tpy-GOs) for the reversible formation of 3D self-assemblies as efficient electrocatalysts for the oxygen reduction reaction (ORR) and as new electrode materials for photocurrent generation and energy storage.

To synthesize tpy-GO, we first prepared GO by the acid oxidation of graphite powder according to the modified Hummers method.[4a,12] Subsequent reactions between an amine-functionalized terpyridine, tpy-NH_2 (see the Supporting Information), and oxygen-containing groups (e.g., carboxy and epoxy groups) in GO in the presence of dicyclohexylcarbodiimide (DCC) led to the formation of tpy-GO (Scheme 1). The tpy-GO thus prepared showed rapid and fully reversible self-assembly with metal ions (e.g., $FeCl_2$). The resultant metal/tpy-GO complexes were shown to be

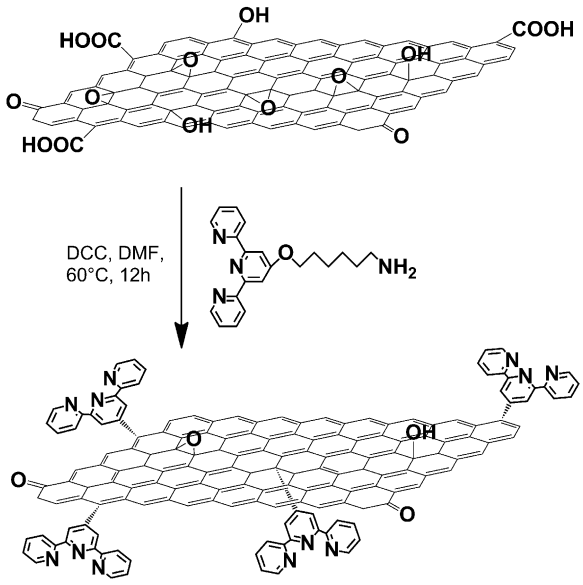

Scheme 1. Schematic illustration of the synthesis of tpy-GO. DMF = *N*,*N*-dimethylformamide.

[*] S. Song, Prof. L. Feng
State Key Laboratory of Chemical Engineering, Department of Chemical and Biological Engineering, Zhejiang University
38 Zheda Road, Hangzhou 310027 (China)
E-mail: fenglf@zju.edu.cn
H. Elbatal, Dr. P. Wang, Dr. C. N. Moorefield, Prof. G. R. Newkome
Department of Polymer Science, University of Akron
Akron, OH (USA)
Dr. Y. Xue, Prof. L. Dai
Center of Advanced Science and Engineering for Carbon (Case4Carbon), Department of Macromolecular Science and Engineering, Case Western Reserve University
10900 Euclid Avenue, Cleveland, OH 44106 (USA)
E-mail: Liming.Dai@case.edu

[**] This research was supported financially by Zhejiang University Caoguangbiao High-Tech Talent Fund and AFOSR (FA9550-12-1-0037) and NSF (GRN CHE-1151991, CMMI-1266295, AIR-IIP-1343270).

Supporting information for this article is available on the WWW under http://dx.doi.org/10.1002/anie.201309641.

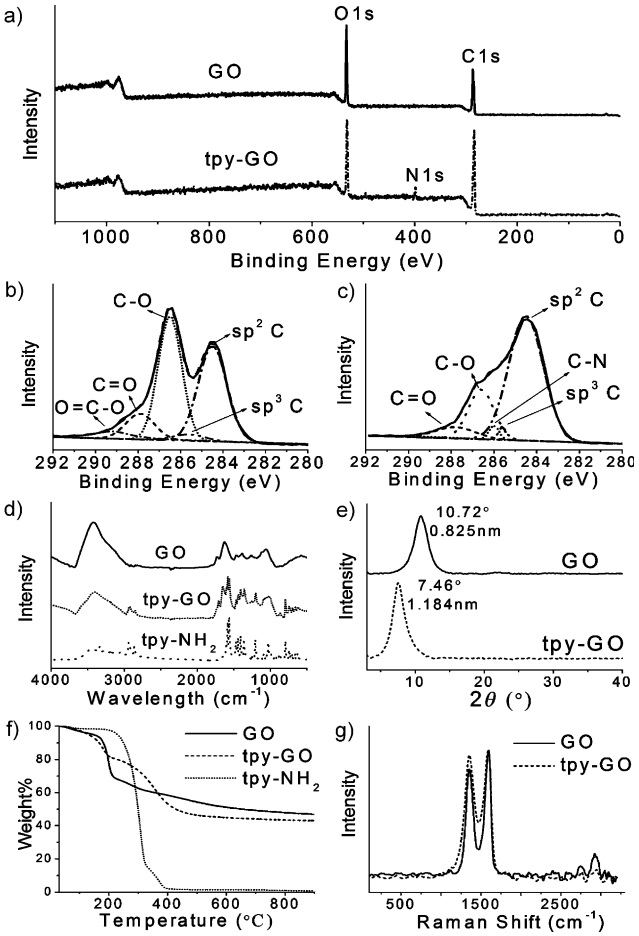

Figure 1. a) XPS spectra of GO and tpy-GO. b,c) High-resolution XPS spectra of C 1s for GO (b) and tpy-GO (c). d) FTIR spectra of GO, tpy-NH_2, and tpy-GO. e) XRD spectra of GO and tpy-GO. f) TGA of GO, tpy-NH_2, and tpy-GO. g) Raman spectra of GO and tpy-GO.

promising for various potential applications, ranging from ORR catalysis and photocurrent generation to energy storage.

Figure 1a shows spectra from X-ray photoelectron spectroscopic (XPS) measurements of GO and tpy-GO. As expected, the spectrum of GO shows only C and O peaks. The appearance of an N 1s (398.8 eV) peak in the XPS spectrum of tpy-GO and the decrease in the intensity ratio of the O 1s to the C 1s peak with respect to that in the spectrum of GO (Figure 1a) indicate the successful grafting of tpy-NH_2 onto GO. The O content dropped from 34.4% for GO to 23.8% for tpy-GO owing to the reaction between carboxy groups of GO with the amine group of tpy-NH_2 (Scheme 1). However, partial reduction of GO as a result of the amidation reaction cannot be ruled out.[13] Figure 1b,c shows the high-resolution C 1s spectra of GO and tpy-GO, respectively. As can be seen, the intensity of the C–O (286.6 eV), C=O (287.8 eV), and O=C–OH peaks (289.2 eV) all decreased significantly upon amidation. The new component C–N at approximately 286.1 eV in the C 1s spectrum of tpy-GO was attributed to the C–N bond between GO and tpy-NH_2 as well as the C–N bonds in the terpyridine group. Fourier transform infrared (FTIR) spectra of GO, tpy-NH_2, and tpy-GO are shown in Figure 1d. The spectrum of GO shows the characteristic peaks at 3420 (C–OH), 1730 (C=O), 1628 (C=C), and 1058 cm^{-1} (C–O). For tpy-GO, the new peak at 1650 cm^{-1} corresponds to the stretching vibration of the amide bonds, thus indicating the occurrence of the amidation reaction. The functionalization of GO with tpy-NH_2 was further confirmed by the appearance of CH_2 stretching vibrations at 2926 and 2856 cm^{-1} along with C=N stretching vibrations at 1580 and 1560 cm^{-1} associated with the newly attached terpyridine moieties.

Figure 1e shows the X-ray diffraction (XRD) spectra of GO and tpy-GO. The broad band for GO ($2\theta = 10.72°$, corresponding to an interlayer distance of approximately 0.825 nm[14]) was downshifted to $2\theta = 7.46°$ (corresponding to an interlayer distance of 1.184 nm) for tpy-GO. The observed increase in the interlayer space indicates further exfoliation of the graphene sheets as induced by functionalization with terpyridine.[15] GO, tpy-NH_2, and tpy-GO were subjected to thermogravimetric analysis (TGA; Figure 1f). Whereas tpy-NH_2 decomposed at around 300 °C, both GO and tpy-GO showed a much smaller weight loss at 180–200 °C associated with the oxygen content in GO.[16,17] Another new thermal band attributable to thermal decomposition of the grafted tpy-NH_2 was observed from 320 to 420 °C for tpy-GO. The functionalization of GO with tpy-NH_2 was further supported by Raman spectra (Figure 1g). Upon the grafting of tpy-NH_2 onto GO sheets, the band-intensity ratio I_D/I_G increased from 1.027 to 1.144, with a concomitant G-band shift from 1598.2 to 1592.7 cm^{-1}. These changes in the Raman spectrum indicate the structure distortions induced by the strong interaction between GO and the tpy functional group.[18] The increase in the ratio of I_D to I_G is due to the formation of a higher number of smaller defect domains as a result of partial reduction induced by the reaction of GO with tpy-NH_2 (see above), whereas the Raman peak shift arises from charge transfer between the newly attached tpy moieties and GO (see below).[5]

The self-assembly behavior of tpy-GO was studied by the addition of $FeCl_2$ to a dispersion of tpy-GO in DMF (Figure 2a, I). Upon the addition of Fe^{2+} ions, a brown precipitate appeared (Figure 2a, II). The observed rapid precipitation indicated the formation of a Fe–tpy-GO self-assembly (Figure 2b). To test the reversibility of the self-assembly process, we transferred the terpyridine–Fe complex in a water/ethanol (1:1) mixture and used ethylenediaminetetraacetic acid (EDTA) as a competing ligand to break up the complex (Figure 2a, III).[19] The tpy-GO was restored well in DMF after treatment with EDTA and could be used again for self-assembly by the readdition of Fe^{2+} ions (Figure 2a, IV). The complexation–decomplexation cycle demonstrated full reversibility of the self-assembly process, as shown schematically in Figure 2b.

The complexation–decomplexation cycle was monitored by UV/Vis spectroscopy. As expected, the tpy-GO exhibited a featureless UV spectrum in DMF (Figure 2c, I). Fe^{2+} ions were then added directly to the tpy-GO solution in the cuvette, and a UV/Vis measurement was made immediately before the complex precipitated. Upon the addition of Fe^{2+} ions, two peaks characteristic of the terpyridine–Fe complex

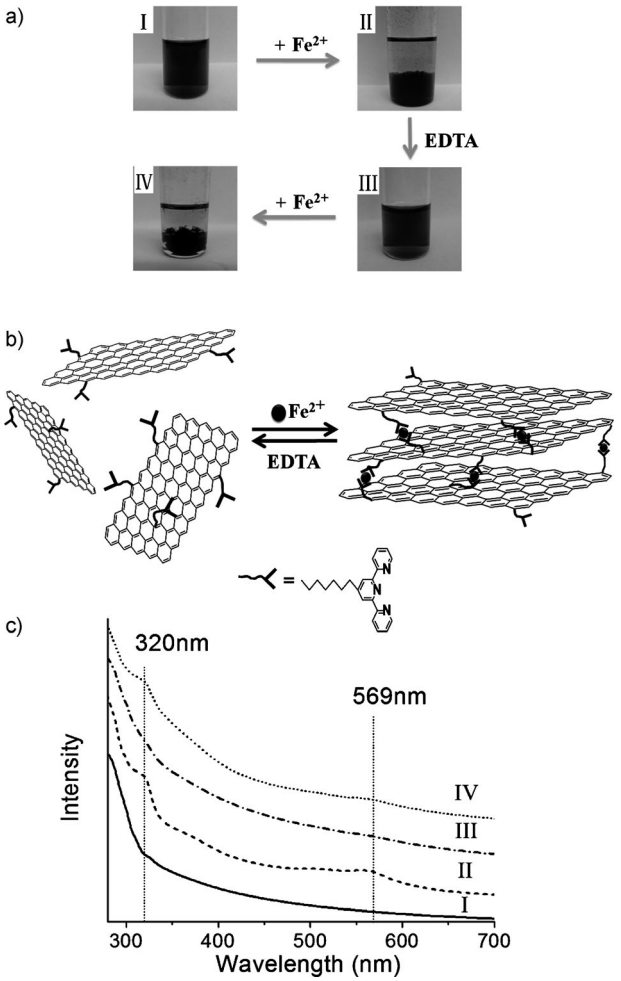

Figure 2. a) Photographs of the dispersion of tpy-GO in DMF during a complexation–decomplexation cycle: I) initial dispersion of tpy-GO in DMF; II) after the addition of $FeCl_2$; III) the complex was collected by filtration, redispersed in a water/ethanol (1:1) mixture, and then treated with EDTA, recollected, and redispersed in DMF for the subsequent test (see the Supporting Information for details); IV) after the addition of $FeCl_2$ (again in DMF). b) Schematic illustration of the complexation–decomplexation (self-assembly) process of tpy-GO. c) UV/Vis spectra of different stages of the complexation–decomplexation cycle: I) initial dispersion of tpy-GO in DMF (3 mL; 0.05 mg mL^{-1}); II) after the addition of two drops of a 0.01 M $FeCl_2$ solution in DMF; III) after treatment with EDTA and redispersion in DMF (3 mL; 0.05 mg mL^{-1}); IV) after the addition of $FeCl_2$ (again in DMF). The UV/Vis spectra have been shifted arbitrarily along the *y* axis for clarity.

appeared at 320 and 569 nm (Figure 2c, II). These peaks are due to ligand transition absorption and metal-to-ligand charge transfer, respectively.[20] After treatment with EDTA, the featureless spectrum observed for tpy-GO was restored (Figure 2c, III), thus indicating the complete decomplexation of the complex. Upon the addition of Fe^{2+} ions again, the two characteristic peaks for the complex reappeared (Figure 2c, IV). Thus, the Fe^{2+}-induced self-assembly of tpy-GO is highly reversible. The formation of the 3D Fe–tpy-GO self-assembly (Figure 2b) was also supported by our preliminary TEM and SEM examination of the Fe–tpy-GO precipitate, with the corresponding tpy-GO sample as a reference (see Figure S1 in the Supporting Information).

Inspired by our previous studies on nitrogen-doped carbon nanomaterials for the ORR,[21,22] we investigated the ORR performance of Fe–tpy-GO by performing linear sweep voltammetric (LSV) measurements on a rotating-disk electrode (RDE) in an O_2-saturated 0.1 M KOH electrolyte solution. Both the tpy-GO ligand and the Fe–tpy-GO complex exhibited high ORR catalytic activities with respect to GO (Figure 3a). The onset potential for the pristine GO

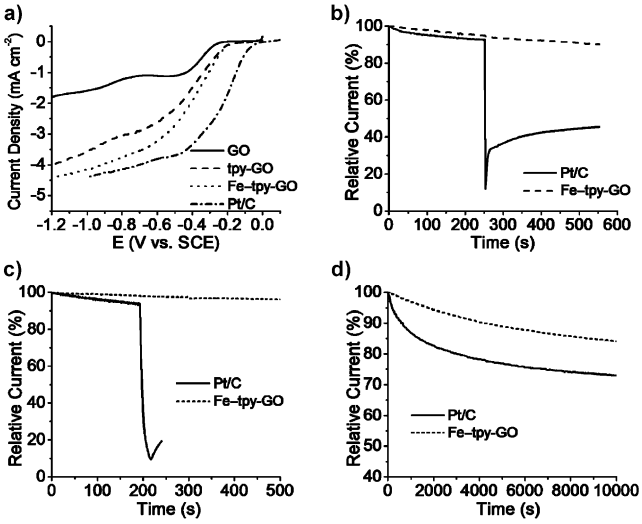

Figure 3. a) Linear sweep voltammetric (LSV) curves for oxygen reduction at the GO, tpy-GO, Fe–tpy-GO, and Pt/C electrodes in an O_2-saturated 0.1 M KOH solution at a scan rate of 10 mV s^{-1}. The electrode rotation speed was 1600 rpm. b–d) Current–time (*i*–*t*) chronoamperometric response for the ORR at the Fe–tpy-GO and Pt/C electrodes in an O_2-saturated 0.1 M KOH solution at −0.3 V versus SCE: b) addition of methanol (3.0 M) at around 250 s; c) addition of CO (9 v/v% mixed with O_2) at around 200 s; d) time dependence at −0.3 V versus SCE at a rotation rate of 900 rpm. SCE = saturated calomel electrode.

was about −0.3 V, whereas the corresponding onset potential for Fe–tpy-GO was shifted positively to about −0.2 V with a concomitant increase in current density. Although the onset potential of the Fe–tpy-GO complex is still not as high as that of the commercial Pt/C electrocatalyst (C2-20, 20% platinum on Vulcan XC-72R; E-TEK), the diffusion-limited current densities of the two catalysts are almost the same. We reported previously that either nitrogen-doping-induced intramolecular charge transfer[21] or polyelectrolyte-adsorption-induced intermolecular charge transfer[22] could improve the ORR activity of graphitic carbon materials. Therefore, the improved ORR activities observed in this study for the Fe–tpy-GO complex over tpy-GO could be attributed mainly to the intermolecular charge transfer between the amide nitrogen atoms (N atoms in tpy) and the partially reduced GO sheet within the self-assembled 3D architecture (Figure 2b). The self-assembled 3D structure played an important role in enhancing the ORR activity,[23] as the Fe–tpy-GO sample after decomplexation with EDTA showed similar ORR

activity to that of tpy-GO. However, possible contributions from metal/tpy complexation within the 3D structure cannot be ruled out.

The Fe–tpy-GO electrode was further subjected to testing for possible cross-over and long-term stability toward the ORR. Figure 3b,c shows the current–time (*i–t*) chronoamperometric responses for the ORR at the Fe–tpy-GO and Pt/C electrodes. Upon the addition of methanol (3.0 M), a sharp decrease in current was observed for the Pt/C electrode (Figure 3b). However, the corresponding amperometric response at the Fe–tpy-GO electrode remained almost unchanged after the addition of methanol, thus indicating that the Fe–tpy-GO electrocatalyst shows higher fuel selectivity toward the ORR than the commercial Pt/C electrocatalyst. The effect of CO poisoning on the electrocatalytic activities of the Fe–tpy-GO and Pt/C electrodes was also examined by the introduction of CO gas into the electrolyte. The Fe–tpy-GO electrode was insensitive to CO, whereas the Pt/C electrode was rapidly poisoned under the same conditions (Figure 3c). Finally, the durability of Fe–tpy-GO and commercial Pt/C electrodes for the ORR was evaluated. The current density of both the Fe–tpy-GO and the Pt/C electrode decreased with time (Figure 3d). However, the Fe–tpy-GO electrode exhibited a much slower decrease than Pt/C, thus indicating that the Fe–tpy-GO electrocatalyst is much more stable than the commercial Pt/C electrode.

To further explore the ORR catalytic activity quantitatively, we determined the electron-transfer number per oxygen molecule involved in the ORR process by the Koutechy–Levich equation (see the Supporting Information). Linear relationships between i^{-1} and $\omega^{-0.5}$ were obtained for GO, tpy-GO, and Fe–tpy-GO (see Figures S4b,d,f). The electron-transfer numbers for the ORR were calculated to be 3.63–3.79 for tpy-GO and 3.63–3.92 for Fe–tpy-GO at the potential ranging from −0.7 to −0.5 V, and are thus much higher than that of the GO electrode (1.39–1.61; see Table S1 in the Supporting Information). The nearly four electron process for the ORR and the relatively high kinetic current density for tpy-GO and Fe–tpy-GO (see Table S1) showed, once again, that tpy-GO and its iron complex are efficient catalysts for the ORR.

Apart from the use of tpy-GO and Fe–tpy-GO as efficient ORR catalysts, the as-synthesized tpy-GO ligand could also complex with ruthenium ions. Our preliminary results showed a photoelectrical response for the Ru–tpy-GO complex, as observed for other similar complexes.[24] Strong, steady, and reversible photocurrent generation was observed from a Ru–tpy-GO/ITO electrode (0.4 cm^2) during on/off cycles of illumination (500 W xenon lamp; Figure 4). Whereas the pristine GO also exhibited a photocurrent response,[25] and the pure ruthenium–terpyridine complex did not,[26] the chemical attachment of tpy to GO significantly reduced the photocurrent through photocurrent quenching and/or resistance enhancement associated with the tpy moieties. Subsequent complexation of tpy-GO with Ru enhanced the photocurrent response to up to twice that of GO, most probably as a result of the improved optical absorption of the dye complex (compare Figure 2c), and hence efficient charge transfer from the excited dye moiety to graphene, in conjugation with

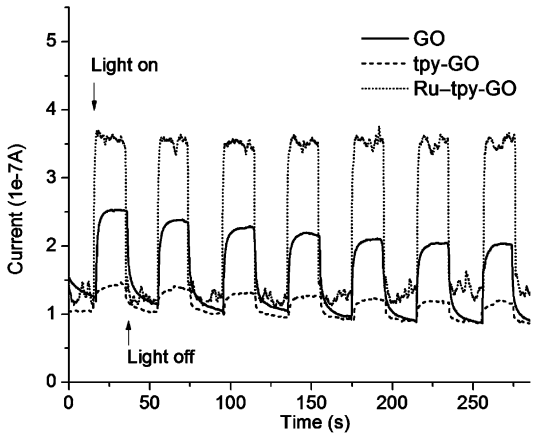

Figure 4. Photocurrent response of GO, tpy-GO, and Ru–tpy-GO in 0.1 M aqueous KCl as observed for the corresponding samples on an indium tin oxide (ITO) electrode (0.4 cm^2) during on/off cycles of illumination (500 W xenon lamp).

improved charge transfer through the self-assembled 3D architecture. Therefore, the Ru–tpy-GO complex could be useful as a new photoelectric material for a variety of applications ranging from photodetection and dye-sensitized solar cells (DSSCs) to H_2 evolution.[27] Furthermore, the newly developed self-assembled 3D metal–tpy-GO complexes were also demonstrated to be useful as promising electrode materials for energy storage (see Figure S5), in analogy with other 3D carbon materials previously reported.[28]

In summary, we have prepared a new class of terpyridine-functionalized graphene by covalently grafting terpyridine groups onto GO. The resultant tpy-GO can undergo rapid and repeatable self-assembly upon the addition of iron ions to form Fe–tpy-GO. Subsequent decomplexation by treatment with EDTA releases the tpy-GO ligand. We have further demonstrated that tpy-GO and Fe–tpy-GO can act as ORR catalysts with superb electrocatalytic activity and superior stability to those of commercial Pt/C catalysts, and are free from CO-poisoning and MeOH-cross-over effects. The self-assembled 3D architecture offers the additional advantage that the metal–tpy-GO complexes can be used as electrode materials for energy conversion (e.g., ORR, photocurrent generation) and storage (e.g., supercapacitors).

Received: November 5, 2013
Published online: December 11, 2013

Keywords: energy conversion · graphene · oxygen reduction reaction · reversible self-assembly · terpyridine

[1] a) M. J. Allen, V. C. Tung, R. B. Kaner, *Chem. Rev.* **2010**, *110*, 132–145; b) D. S. Yu, L. M. Dai, *J. Phys. Chem. Lett.* **2010**, *1*, 467–470; c) L. T. Qu, Y. Liu, J. B. Baek, L. M. Dai, *ACS Nano* **2010**, *4*, 1321–1326; d) Y. Liu, D. S. Yu, C. Zeng, Z. C. Miao, L. M. Dai, *Langmuir* **2010**, *26*, 6158–6160.

[2] L. Yan, Y. B. Zheng, F. Zhao, S. J. Li, X. F. Gao, B. Q. Xu, P. S. Weiss, Y. L. Zhao, *Chem. Soc. Rev.* **2012**, *41*, 97–114.

[3] S. Y. Bae, I. Y. Jeon, J. Yang, N. Park, H. S. Shin, S. Park, R. S. Ruoff, L. M. Dai, J. B. Baek, *ACS Nano* **2011**, *5*, 4974 – 4980.
[4] a) Y. H. Xue, H. Chen, D. S. Yu, S. Y. Wang, M. Yardeni, Q. B. Dai, M. M. Guo, Y. Liu, F. Lu, J. Qu, L. M. Dai, *Chem. Commun.* **2011**, *47*, 11689 – 11691; b) D. S. Yu, E. Nagelli, R. Naik, L. M. Dai, *Angew. Chem.* **2011**, *123*, 6705 – 6708; *Angew. Chem. Int. Ed.* **2011**, *50*, 6575 – 6578.
[5] L. Dai, *Acc. Chem. Res.* **2013**, *46*, 31 – 42, and references therein.
[6] Y. X. Xu, G. Q. Shi, *J. Mater. Chem.* **2011**, *21*, 3311 – 3323.
[7] E. C. Constable, *Chem. Soc. Rev.* **2007**, *36*, 246 – 253.
[8] P. S. Wang, C. N. Moorefield, G. R. Newkome, *Angew. Chem.* **2005**, *117*, 1707 – 1711; *Angew. Chem. Int. Ed.* **2005**, *44*, 1679 – 1683.
[9] M. Chiper, D. Fournier, R. Hoogenboom, U. S. Schubert, *Macromol. Rapid Commun.* **2008**, *29*, 1640 – 1647.
[10] a) S. H. Hwang, C. N. Moorefield, L. M. Dai, G. R. Newkome, *Chem. Mater.* **2006**, *18*, 4019 – 4024; b) Y. X. Pan, B. Tong, J. B. Shi, W. Zhao, J. B. Shen, J. G. Zhi, Y. P. Dong, *J. Phys. Chem. C* **2010**, *114*, 8040 – 8047; c) Y. Lee, H. J. Song, H. S. Shin, H. J. Shin, H. C. Choi, *Small* **2005**, *1*, 975 – 979.
[11] P. R. Andres, U. S. Schubert, *Adv. Mater.* **2004**, *16*, 1043 – 1068.
[12] W. S. Hummers, R. E. Offeman, *J. Am. Chem. Soc.* **1958**, *80*, 1339 – 1339.
[13] Y. H. Xue, Y. Liu, F. Lu, J. Qu, H. Chen, L. M. Dai, *J. Phys. Chem. Lett.* **2012**, *3*, 1607 – 1612.
[14] I. K. Moon, J. Lee, R. S. Ruoff, H. Lee, *Nat. Commun.* **2010**, *1*, 73 – 79.
[15] Q. Wu, Y. Q. Sun, H. Bai, G. Q. Shi, *Phys. Chem. Chem. Phys.* **2011**, *13*, 11193 – 11198.
[16] S. Niyogi, E. Bekyarova, M. E. Itkis, J. L. McWilliams, M. A. Hamon, R. C. Haddon, *J. Am. Chem. Soc.* **2006**, *128*, 7720 – 7721.
[17] Z. Y. Lin, Y. G. Yao, Z. Li, Y. Liu, Z. Li, C. P. Wong, *J. Phys. Chem. C* **2010**, *114*, 14819 – 14825.
[18] S. Niyogi, E. Bekyarova, M. E. Itkis, H. Zhang, K. Shepperd, J. Hicks, M. Sprinkle, C. Berger, C. N. Lau, W. A. Deheer, E. H. Conrad, R. C. Haddon, *Nano Lett.* **2010**, *10*, 4061 – 4066.
[19] H. Hofmeier, U. S. Schubert, *Macromol. Chem. Phys.* **2003**, *204*, 1391 – 1397.
[20] C. F. Zhang, H. X. Huang, B. Liu, M. Chen, D. J. Qian, *J. Lumin.* **2008**, *128*, 469 – 475.
[21] K. P. Gong, F. Du, Z. H. Xia, M. Durstock, L. M. Dai, *Science* **2009**, *323*, 760 – 764.
[22] S. Y. Wang, D. S. Yu, L. M. Dai, D. W. Chang, J. B. Baek, *ACS Nano* **2011**, *5*, 6202 – 6209.
[23] Y. H. Xue, D. S. Yu, L. M. Dai, R. G. Wang, D. Q. Li, A. Roy, F. Lu, H. Chen, Y. Liu, J. Qu, *Phys. Chem. Chem. Phys.* **2013**, *15*, 12220 – 12226.
[24] A. Wojcik, P. V. Kamat, *ACS Nano* **2010**, *4*, 6697 – 6706.
[25] J. Loomis, B. Panchapakesan, *Nanotechnology* **2012**, *23*, 265203.
[26] K. Jiang, H. Xie, W. Zhan, *Langmuir* **2009**, *25*, 11129 – 11136.
[27] P. V. Kamat, *J. Phys. Chem. Lett.* **2010**, *1*, 520 – 527.
[28] F. Du, D. S. Yu, L. M. Dai, S. Ganguli, V. Varshney, A. K. Roy, *Chem. Mater.* **2011**, *23*, 4810 – 4816.

